Astron. Astrophys. 332, 909–927 (1998)

ASTRONOMY AND ASTROPHYSICS

SZ Camelopardalis – an early-type eclipsing binary embedded in a multiple system⋆

Reinald Lorenz[1], **Pavel Mayer**[2], **and Horst Drechsel**[1]

[1] Dr. Remeis-Sternwarte Bamberg, Astronomisches Institut der Universität Erlangen-Nürnberg, Sternwartstraße 7, D-96049 Bamberg, Germany
[2] Astronomical Institute, Charles University, Švédská 8, CZ-150 00 Praha 5, Czech Republic

Received 14 October 1997 / Accepted 20 November 1997

This paper is dedicated to the memory of Professor Dr. Jürgen Rahe, who died in a tragic accident on June 18, 1997. During more than a decade at Remeis Observatory Bamberg, Dr. Rahe has greatly promoted and contributed to close binary research.

Abstract. We present a spectroscopic and photometric analysis of a complex multiple system: the early-type eclipsing binary SZ Cam (O9 IV + B0.5 V) is physically bound to a third body, which itself is a close binary; this quadruple system has a visual companion, which shows evidence for duplicity as well. A careful deconvolution of spectral lines in our CCD spectra yields rv curves of the SB2 system (K_1 = 180 km s^{-1}, K_2 = 261 km s^{-1}; $P = 2\overset{\mathrm{d}}{.}6984$) and of its SB1 companion ($K_{1,\mathrm{T}}$ = 25 km s^{-1}; $P = 2\overset{\mathrm{d}}{.}7966$). UBV light curves of Kitamura & Yamasaki (1970) are reanalyzed and absolute dimensions of the eclipsing pair are derived. Both components of this close detached binary are overluminous for their masses. The photometric solution suggests third light of $\approx 20 - 30\,\%$, which confirms the spectroscopic and speckle interferometric detection (Mason 1995) of the third component. The observed light time effect encompasses the long period range to $\sim$ 50-60 years. Comparison of calculated orbits with the speckle interferometric result yields a distance of 1050 pc, which is $\sim 10\,\%$ larger than the value derived from the absolute bolometric magnitude, and $\sim 20\,\%$ above the photometric distance of the open cluster NGC 1502. The minimum mass of the third component is 20-30 $M_\odot$, depending on the long orbital period and inclination assumed. This high mass supports the binary nature of the third body. An analysis of the spectra of the visual companion ADS 2984 A confirms its binarity.

Key words: stars: individual: SZ Camelopardalis – binaries: eclipsing – binaries: spectroscopic – stars: early-type – stars: fundamental parameters

Send offprint requests to: R. Lorenz

⋆ Based on observations collected at the German-Spanish Astronomical Centre, Calar Alto, operated by the Max-Planck-Institut für Astronomie, Heidelberg, jointly with the Spanish National Commission for Astronomy

1. Introduction

The early-type eclipsing binary SZ Cam (HD 25638; SAO 13030; HR 1260; BD+61°676N; ADS 2984 B) is the northern component of a visual double star consisting of two components with nearly equal brightness and spectral type, which are the brightest members of the galactic cluster NGC 1502. The separation of 18″ was already measured by W. Struve in 1830. The close spatial coincidence of two very similar stars repeatedly led to confusion with the proper identification of the visual companions (e.g., SZ Cam was erroneously designated as ADS 2984 A in the Bright Star Catalogue, and was also misidentified as HD 25639 in the BSC Supplement, while in all other sources it is cross-referenced with HD 25638).

SZ Cam was first recognized as a spectroscopic binary by Plaskett (1924). The spectral type is B0 II-III according to Morgan et al. (1955), whereas Budding (1975) gives O9.5 V. The V magnitude reaches 6.9 at maximum. The photometric variability of SZ Cam was discovered by Guthnick & Prager (1930). The visual double star was selected as a target for photographic photometry with a long focus refractor by Wesselink (1941), because the observations appeared promising due to the similarity of the two visual components. Consisting of more than 12 000 individual measurements, his eclipse light curve is one of the most accurate photographic light curves ever obtained. Later photoelectric light curves were measured by Kitamura & Yamasaki (1970) in UBV, by Polushina and Gorda in BV and UBV (see Polushina & Pustylnik 1994), and by Chochol (1980) in two intermediate passband filters; also smaller fractions of the light curve were obtained by Delgado (1993) in uvby, and by Irsmambetova (1994). From published times of minima it has been evident that the orbital period of the close binary is changing (Chochol 1977); the $O - C$ variations were first interpreted as light time effect by Mayer (1987).

Spectroscopy was as well attempted by several authors, e.g. by Budding (1975) and Chochol (1980). However, the results were not much satisfying: in photographic spectrograms, the presence of secondary lines was uncertain and namely the derived mass ratio was in discrepancy with the relative luminosities of the components as determined from photometry. Interaction

effects like mass exchange and presence of circumstellar matter were appealed to account for such inconsistencies.

Using new times of minima and Coudé CCD spectroscopy, Mayer et al. (1994; hereafter: Paper I) proved the presence of a third component in the eclipsing system. Based on this knowledge the older data could be reasonably interpreted, and the stellar parameters of both members of the eclipsing system appeared quite reliable. Shortly after Paper I was published, the third component was independently discovered by speckle interferometry (Mason 1994; 1995).

During several observing seasons at the Calar Alto Observatory, we obtained new CCD spectra, which were used to construct the radial velocity curves of both SZ Cam components (Sect. 2.3). After a thorough deconvolution of the spectral line blends consisting of the primary and secondary components of the eclipsing pair and the third body lines, it was also possible to prove that the third body in the system is a single-lined spectroscopic binary itself, with a period by chance very similar to that of SZ Cam (Sect. 2.4). Given the knowledge of appreciable third light, the light curve of Kitamura & Yamasaki (1970) was reanalyzed using the MORO light curve solution code (Drechsel et al. 1995), which accounts for radiation pressure effects in early-type close binaries (Sect. 3). Orbital parameters and other properties of the third body are further discussed in connection with the speckle interferometric measurements (Sect. 4).

Plaskett (1924) also noted that the radial velocity of the visual component ADS 2984 A was variable. We obtained several spectra of this star and confirmed his suspicion (Sect. 5). Therefore, ADS 2984 is actually a rare case of a sextuple system, for which the various kinds of multiplicity can be inferred from its visual binarity, photometry (analysis of eclipses and light time effect), spectroscopy, and speckle interferometry.

2. Spectroscopy

2.1. Observations and data reduction

A total of 39 spectra were taken with the Coudé spectrograph of the 2.2m telescope at the DSAZ Calar Alto Observatory during three observing seasons in January 1993, December 1993, and July 1995. The f/3 camera and grating #3 in order 2 and the CCDs Tek #6 (1993) and Tek #13 (1995) were used, both consisting of 1024 × 1024 px. No CCD pixel binning was applied. The linear dispersion was 8.5 Å mm^{-1}, and the resolving power was in the range of 24 000 to 32 000. The useful wavelength interval extended over 210 Å and mostly covered the regions from Hβ to He I 5016 and from Hα to He I 6678. In order to measure equivalent widths of He II lines, one additional spectrum was taken containing the lines He II 4542 and 4686. Mean exposure times of 30 to 60 minutes yielded signal-to-noise ratios of about 140 to 200, and allowed for a clear deconvolution of the line blends of this multiple system. A journal of spectra is given in Table 1.

The data reduction was performed with the ESO Munich Image Data Analysis System (MIDAS). In order to achieve a reliable wavelength calibration, which is crucial for the derivation of precise radial velocities, immediately before or after each SZ Cam exposure a Th-Ar comparison spectrum was taken. Each object spectrum of SZ Cam was wavelength-calibrated with its corresponding Th-Ar spectrum yielding accurate individual dispersion relations.

At first glance, obviously the most prominent lines besides Hα and Hβ are the He I lines (4713, 4922, 5016, and 6678) and He II 4686; He II 4542 is much weaker. Besides He, many lines of other elements can be identified, e.g. O II, C III, and N III, which are responsible for the strong blended feature around 4650Å. Furthermore, five Si III lines (4553, 4568, 4575, 4820,

Table 1. Journal of spectra

hel. JD -2 440 000 [a]	ϕ [b]	$t\,(sec)$ [c]	spectral range (Å)
8999.37424	0.840	1800	6515-6725
8999.54507	0.903	1800	4790-5000
8999.62701	0.933	2400	4835-5045
8999.65409	0.943	1200	4835-5045
9000.27975	0.175	1800	4835-5045
9000.30545	0.185	1800	4835-5045
9000.45752	0.241	1800	6515-6725
9000.63321	0.306	2700	6515-6725
9001.30748	0.556	1800	4820-5030
9001.33387	0.566	1800	6515-6725
9001.49289	0.625	1500	4820-5030
9001.63594	0.678	2100	6515-6725
9002.30604	0.926	1800	6515-6725
9002.53798	0.012	1800	6515-6725
9324.32654	0.264	3600	6510-6720
9324.42585	0.301	3600	4820-5030
9324.47377	0.318	3000	4820-5030
9324.51474	0.334	2700	4820-5030
9324.55988	0.350	1800	6510-6720
9324.58696	0.360	1200	6510-6720
9325.35502	0.645	2100	4820-5030
9325.59460	0.734	1800	6510-6720
9325.67724	0.764	1800	6510-6720
9325.70710	0.776	2100	4820-5030
9325.73974	0.788	2700	4820-5030
9328.26752	0.724	1800	6510-6720
9328.29391	0.734	1800	6510-6720
9328.49877	0.810	3605	4820-5030
9328.63349	0.860	2100	6510-6720
9328.66474	0.872	1840	6510-6720
9328.72794	0.895	1800	6510-6720
9329.45085	0.163	1800	4820-5030
9329.47724	0.173	1800	6510-6720
9330.27168	0.467	1500	6510-6720
9331.26890	0.837	1800	4820-5030
9908.62059	0.798	2704	4830-5040
9908.65670	0.811	2701	4830-5040
9909.66160	0.184	2268	4830-5040
9913.66386	0.667	2700	4525-4735

[a] time of mid-exposure;
[b] orbital phase of the eclipsing binary according to:
hel. JD 2448932$^{\rm d}$.3474 + 2$^{\rm d}$.698393 · E (see Paper I);
[c] exposure time.

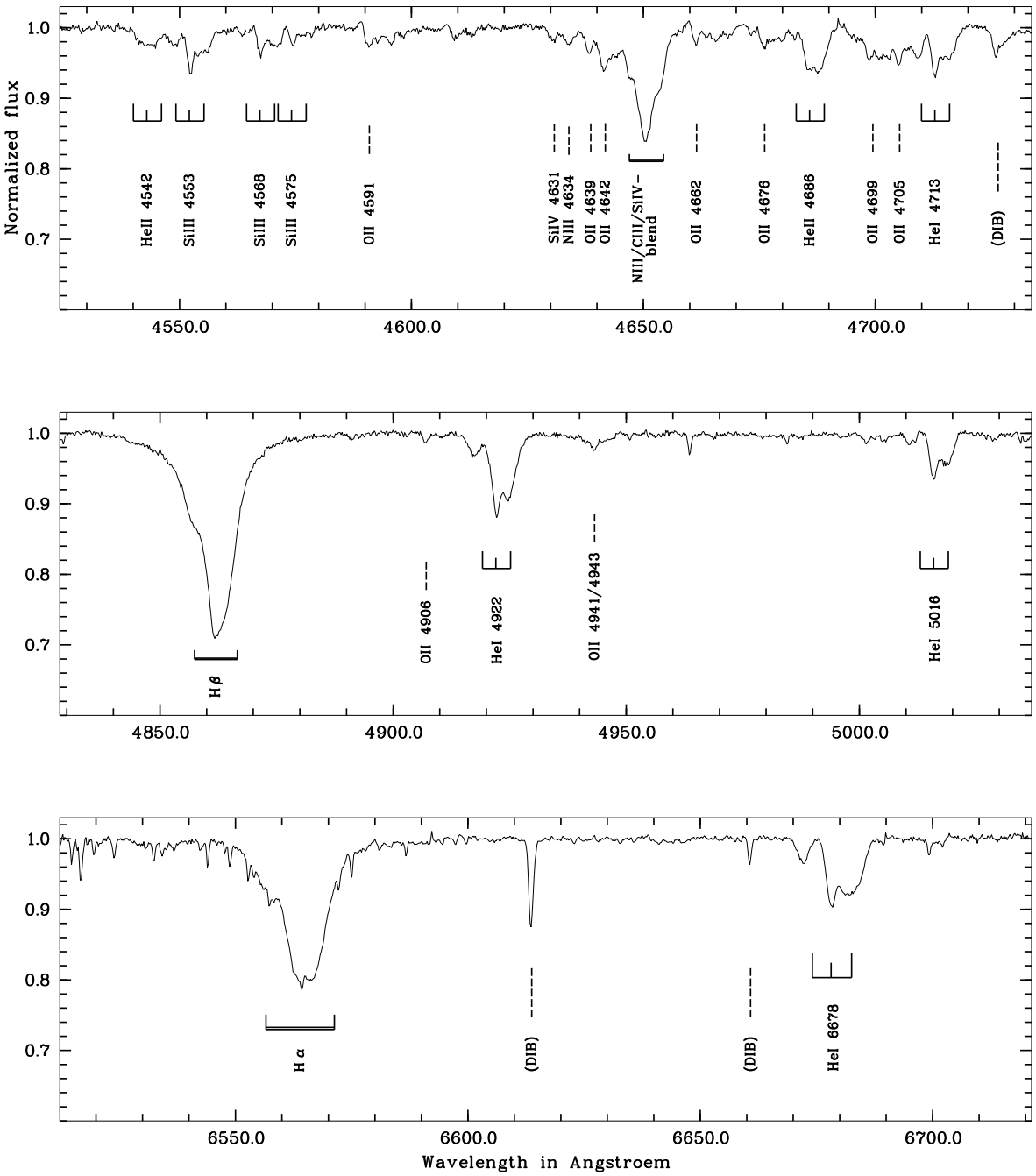

Fig. 1. Typical spectra of SZ Cam obtained with the Coudé spectrograph at the 2.2m telescope of Calar Alto Observatory. The spectra were taken at orbital phases 0.67 (above), 0.81 (middle) and 0.73 (below). Helium and silicon lines clearly show the Doppler separation into three line components (primary red-shifted, secondary blue-shifted, third body line amidst primary and secondary line). Some more prominent spectral lines are indicated as well as diffuse interstellar bands (DIB).

and 4829) and one weak Si IV line (4631) are present. Close to quadrature phases, He I, He II, and Si III lines of the primary and secondary close binary components as well as of the third body can easily be recognized, whereas in the case of Si IV, N III, C III, and O II, only lines of the third body can be detected. This is due to the fact that the third component's lines are much sharper than those of the eclipsing pair and clearly stand out against the continuum noise. As an example, Fig. 1 shows three spectra of SZ Cam taken in different spectral ranges at orbital phases 0.67, 0.81, and 0.73.

2.2. Radial velocity measurements

The radial velocity curve of SZ Cam is based on 31 spectra collected near quadrature phases (i.e. from phases 0.16 to 0.36

and 0.63 to 0.89). For the computation of phases, the following ephemeris as suggested in Paper I was applied:

Pri. min.: hel. JD $2448932^{\rm d}.3474 + 2^{\rm d}.698393 \cdot E$.

Following Kitamura & Yamasaki (1970), and in accordance with our photometric solution, the orbital eccentricity can be assumed to be zero. For the determination of radial velocities of the different stellar components, the He I lines 4713, 4922, 5016, and 6678 and the He II lines 4542 and 4686 were used. The radial velocities derived from these lines could be complemented by those of Si III 4553, 4568, and 4575, which appear in the spectrum taken at JD $2449913^{\rm d}.664$. Due to a blend of the primary Si III 4568 and the secondary Si III 4575 components, the corresponding radial velocities were discarded. Because of their broad profiles and severe blending, H lines were not used for radial velocity determinations. Moreover, the Si IV, N III, C III, and O II lines were rejected due to their weakness, blending with other features, or because of the fact that in some cases their radial velocities showed systematic deviations compared with those derived from, e.g., He lines (cf. Mayer et al. 1997).

The line features were fitted with individual Gaussian profiles for each stellar component using the Newton-Raphson method for the optimization of the following free parameters: central wavelength, full width at half maximum (FWHM), and amplitudes of the Gaussian functions. As the third body lines are always blended with those of the primary, and in out-of-quadrature phases also with those of the secondary, a simultaneous fit with three Gaussian functions was required. In the spectra containing the He I 6678 line, an additional absorption feature at about 6672 Å was clearly visible. As it was always blended with the primary or secondary lines, it was fitted with an extra Gaussian profile. The origin of this feature could not be clarified, but possibly it is of interstellar nature.

Using this set of three (or in the case of He I 6678: four) different Gaussian profiles, it was possible to disentangle the more or less strongly blended lines (depending on orbital phase), and to derive an accurate radial velocity curve. Radial velocities were calulated including the barycentric correction for the mass center of the solar system. The results for the eclipsing binary components and the third body are listed in Table 2. Typical line features and Gaussian fits of helium lines are shown in Fig. 2.

2.3. The radial velocity curve of the eclipsing pair

Our radial velocity curve of the eclipsing pair of SZ Cam is based on 100 individual radial velocity measurements. The radial velocity curves of the primary and the secondary components were first separately fitted with sine functions $\gamma_{0,i} + A_i \cdot \sin\phi$ ($i = 1, 2$ for the primary and secondary components, respectively) and using the Newton-Raphson method to optimize the free parameters (amplitudes A_i and systemic velocities $\gamma_{0,i}$); ϕ denotes the orbital phase. We obtained

$A_1 = -179.6$ km s^{-1}, $\gamma_{0,1} = 5.7$ km s^{-1} and

$A_2 = 258.2$ km s^{-1}, $\gamma_{0,2} = -11.5$ km s^{-1}.

The systemic velocities $\gamma_{0,1}$ and $\gamma_{0,2}$ differ by 17.18 km s^{-1}, which obviously cannot be a real effect. However, such inconsistencies are a well known and so far unsolved problem when analyzing radial velocities of close binaries (cf. Mayer et al. 1991). To obtain consistent radial velocity curves for both components, the arithmetic mean of $\gamma_{0,1}$ and $\gamma_{0,2}$ was used as systemic velocity of the eclipsing pair:

$\gamma_0 = -2.9$ km s^{-1} $\pm$ 1.6 km s^{-1}.

The given error is due to the uncertainty of the $\gamma_{0,1}$ and $\gamma_{0,2}$ fits, whereas the real error is probably fairly larger and lies in the range of $|\gamma_{0,1} - \gamma_{0,2}|$.

Now each of the radial velocity curves of both components were re-fitted with a sine function

$\gamma_0 + K_i \sin\phi$,

with γ_0 as fixed parameter and $K_i = K_1, K_2$ representing the radial velocity amplitudes of the primary and the secondary components, respectively, as adjustable quantities. The result was

$K_1 = 180.2$ km s^{-1} $\pm$ 2.0 km s^{-1};

$K_2 = 261.2$ km s^{-1} $\pm$ 3.8 km s^{-1},

and therefore the spectroscopic mass ratio of SZ Cam amounts to:

$q_{\rm spec} = K_1/K_2 = M_2/M_1 = 0.690 \pm 0.015$.

The given error limit represents the formal fit errors. The differences between A_1 and K_1 as well as between A_2 and K_2 are very small, which justifies the use of an average systemic velocity in the way described above.

It should be emphasized that $q_{\rm spec} = 0.690$ is remarkably different from any mass ratio previously published by other authors, who did not take the presence of a third body into consideration (e.g., Chochol (1980) gives $q_{\rm spec} = 0.25$). Obviously, this difference has crucial implications on the determination of the masses of the stellar components and the system configuration.

According to the derived K_i values, the semi-major axes come out as

$a_1 \sin i = 9.60 \pm 0.11$ R$_\odot$ and $a_2 \sin i = 13.92 \pm 0.20$ R$_\odot$.

Fig. 3 shows the radial velocity curves of the primary and secondary components and the fitted sine functions.

2.4. The radial velocity curve of the third body

The radial velocity variations of the third body already suspected in Paper I could clearly be confirmed. Based on 51 radial velocity measurements in 31 of our high-resolution spectra, it was therefore possible to proof the binarity of the third body.

As the deconvolution of three strongly blended spectral lines is a quite complicated task, and the radial velocity amplitude of

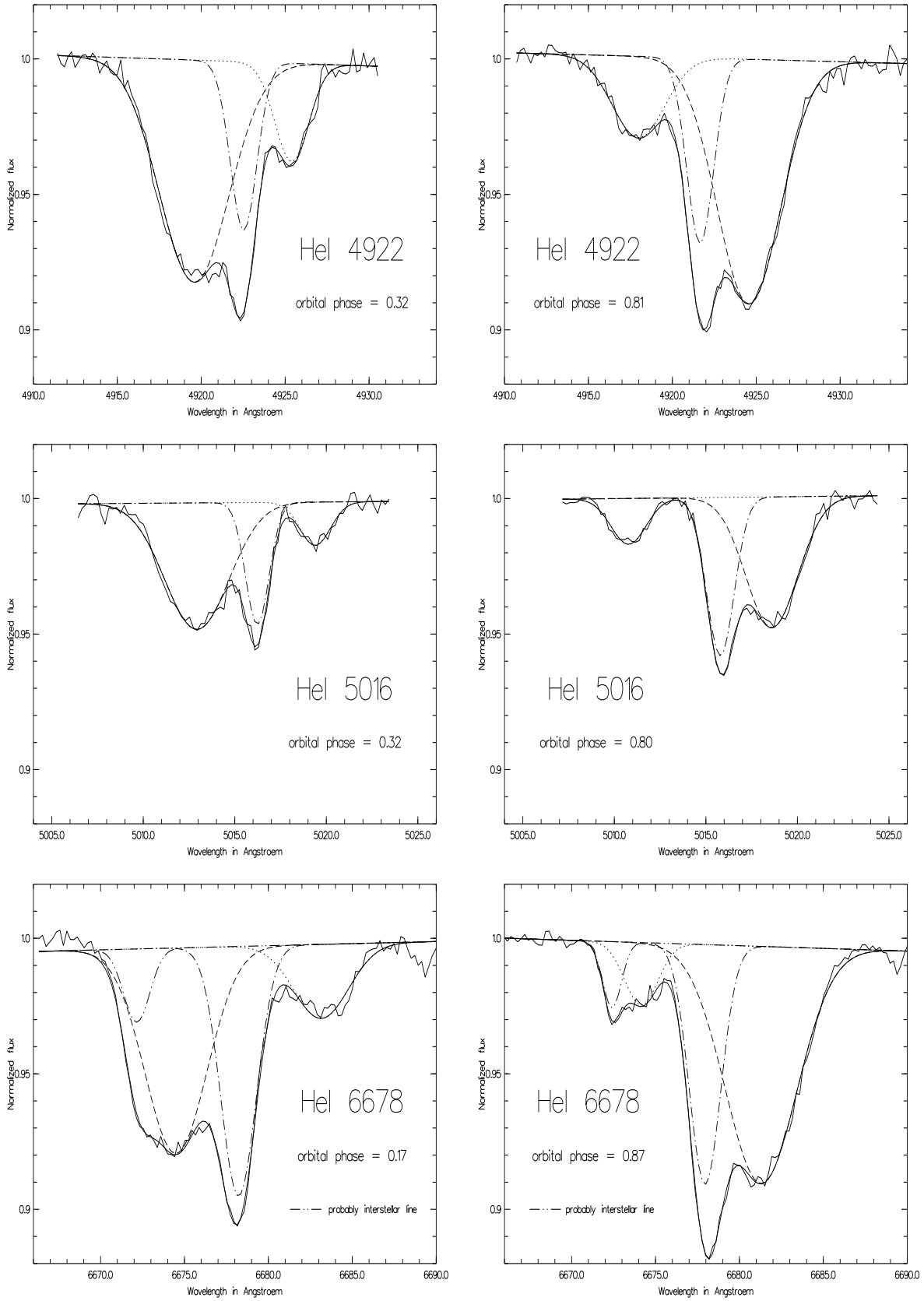

Fig. 2. Typical profiles of He I 4922, 5016, and 6678 spectral lines around both quadrature phases. The fitted Gaussian functions are drawn as dashed, dotted, and dash-dotted lines for the primary and secondary component and the third body, respectively. The resulting fit curve is shown as solid line. In the case of He I 6678, an additional feature, probably of interstellar origin, is shown as dash-double-dotted line.

Table 2. Radial velocities of eclipsing binary components and third body

Line	hel. JD -2 440 000	ϕ [a]	v_1 (km s^{-1})	Δv_1 [b]	v_2 (km s^{-1})	Δv_2 [c]	ϕ_T [d]	v_3 (km s^{-1})	Δv_3 [e]
He I 4713	9913.664	0.667	165.9	4.5	-229.8	2.4	0.401	-8.4	1.4
He I 4922	9000.280	0.175	-129.7	5.8	205.3	6.4	0.793	36.6	2.5
	9000.305	0.185	-132.8	4.9	218.0	4.9	0.803	38.9	2.0
	9001.493	0.625	137.8	4.4	-172.9	10.2	0.227	-15.7	1.9
	9324.426	0.301	-152.2	4.2	220.0	4.3	0.702	33.6	1.8
	9324.474	0.318	-141.9	4.8	212.0	3.5	0.719	37.8	2.0
	9324.515	0.334	-135.9	4.6	206.4	4.2	0.733	35.9	2.1
	9325.355	0.645	153.3	3.7	-183.5	9.0	0.034	-0.8	1.5
	9325.707	0.776	163.9	3.4	-260.1	5.7	0.160	-21.3	1.9
	9325.740	0.788	171.7	3.2	-263.8	4.8	0.171	-21.3	1.8
	9328.499	0.810	153.8	3.3	-247.0	4.1	0.158	-22.9	1.5
	9329.451	0.163	-164.0	7.1	191.7	4.8	0.498	-2.6	2.3
	9331.269	0.837	148.6	3.8	-214.5	7.6	0.148	-19.6	1.8
	9908.621	0.798	181.7	4.1	-261.1	3.5	0.598	10.5	2.0
	9908.657	0.811	182.9	4.2	-249.5	3.8	0.611	13.6	2.0
	9909.662	0.184	-158.5	5.9	197.8	5.4	0.970	6.6	2.5
He I 5016	9000.280	0.175	-165.5	4.9	229.0	8.1	0.793	35.9	2.2
	9000.305	0.185	-166.8	4.6	245.7	7.6	0.803	37.7	2.1
	9001.493	0.625	153.6	3.8	-218.8	7.1	0.227	-9.0	1.8
	9324.426	0.301	-177.1	3.2	235.9	5.9	0.702	32.7	1.7
	9324.474	0.318	-162.9	3.3	223.2	4.6	0.719	34.4	1.6
	9324.515	0.334	-155.1	3.4	215.5	4.6	0.733	36.1	1.6
	9325.355	0.645	168.0	3.5	-225.9	5.1	0.034	8.4	1.7
	9325.707	0.776	181.9	3.1	-284.9	5.8	0.160	-10.0	1.9
	9325.740	0.788	186.7	3.3	-282.5	5.4	0.171	-7.6	2.2
	9328.499	0.810	171.3	3.2	-269.8	4.9	0.158	-14.0	1.8
	9329.451	0.163	-169.6	4.5	218.9	5.4	0.498	1.3	1.7
	9331.269	0.837	163.3	3.3	-256.9	5.1	0.148	-11.9	1.7
	9908.621	0.798	188.3	2.9	-279.1	3.5	0.598	20.4	1.4
	9908.657	0.811	191.3	3.5	-271.3	5.1	0.611	24.0	1.8
	9909.662	0.184	-173.6	3.8	226.3	4.1	0.970	8.7	1.6
He I 6678	8999.374	0.840	158.9	3.0	-187.6	3.8	0.470	8.6	1.0
	9000.458	0.241	-168.8	3.4	258.6	4.2	0.857	25.6	1.3
	9000.633	0.306	-163.9	3.6	236.0	3.9	0.919	12.0	1.4
	9001.636	0.678	158.5	2.7	-241.5	4.6	0.278	-14.3	1.1
	9324.327	0.264	-169.2	3.3	258.1	5.1	0.666	25.6	1.8
	9324.560	0.350	-138.6	3.0	193.6	4.2	0.749	29.3	1.3
	9324.587	0.360	-136.4	4.2	186.4	5.7	0.759	27.0	1.8
	9325.595	0.734	171.1	2.8	-284.5	6.2	0.119	-10.7	1.2
	9325.677	0.764	172.8	2.7	-290.4	5.7	0.149	-14.4	1.2
	9328.268	0.724	173.0	3.2	-279.9	6.3	0.075	-4.7	1.3
	9328.294	0.734	174.8	2.7	-301.1	6.3	0.085	-7.9	1.1
	9328.633	0.860	142.5	2.4	-192.0	4.5	0.206	-15.1	0.8
	9328.665	0.872	134.4	2.6	-185.7	7.8	0.217	-15.1	0.8
	9328.728	0.895	118.2	2.8	-175.9	3.9	0.240	-16.1	0.8
	9329.477	0.173	-165.2	4.0	223.6	3.9	0.507	2.7	1.6
He II 4542	9913.664	0.667	183.0	27.1	-180.0	44.9	0.401	6.8	21.1
He II 4686	9913.664	0.667	153.4	5.7	-187.0	4.7	0.401	-8.5	3.6
Si III 4553	9913.664	0.667	154.3	8.3	-233.6	6.5	0.401	-8.4	1.8
Si III 4568	9913.644	0.667			-237.3	9.5	0.401	-8.9	2.9
Si III 4575	9913.664	0.667	164.1	15.1			0.401	-13.5	3.1

[a] eclipsing binary phases computed with ephemeris: hel. JD 2448932.^{d}3474 + 2.^{d}698393 · E;
[b] mean fit error of v_1 in km s^{-1}
[c] mean fit error of v_2 in km s^{-1}
[d] phases of binary T ("third body") computed with ephemeris: hel. JD 2448998.^{d}0608 + 2.^{d}7966 · E;
[e] mean fit error of v_3 in km s^{-1}

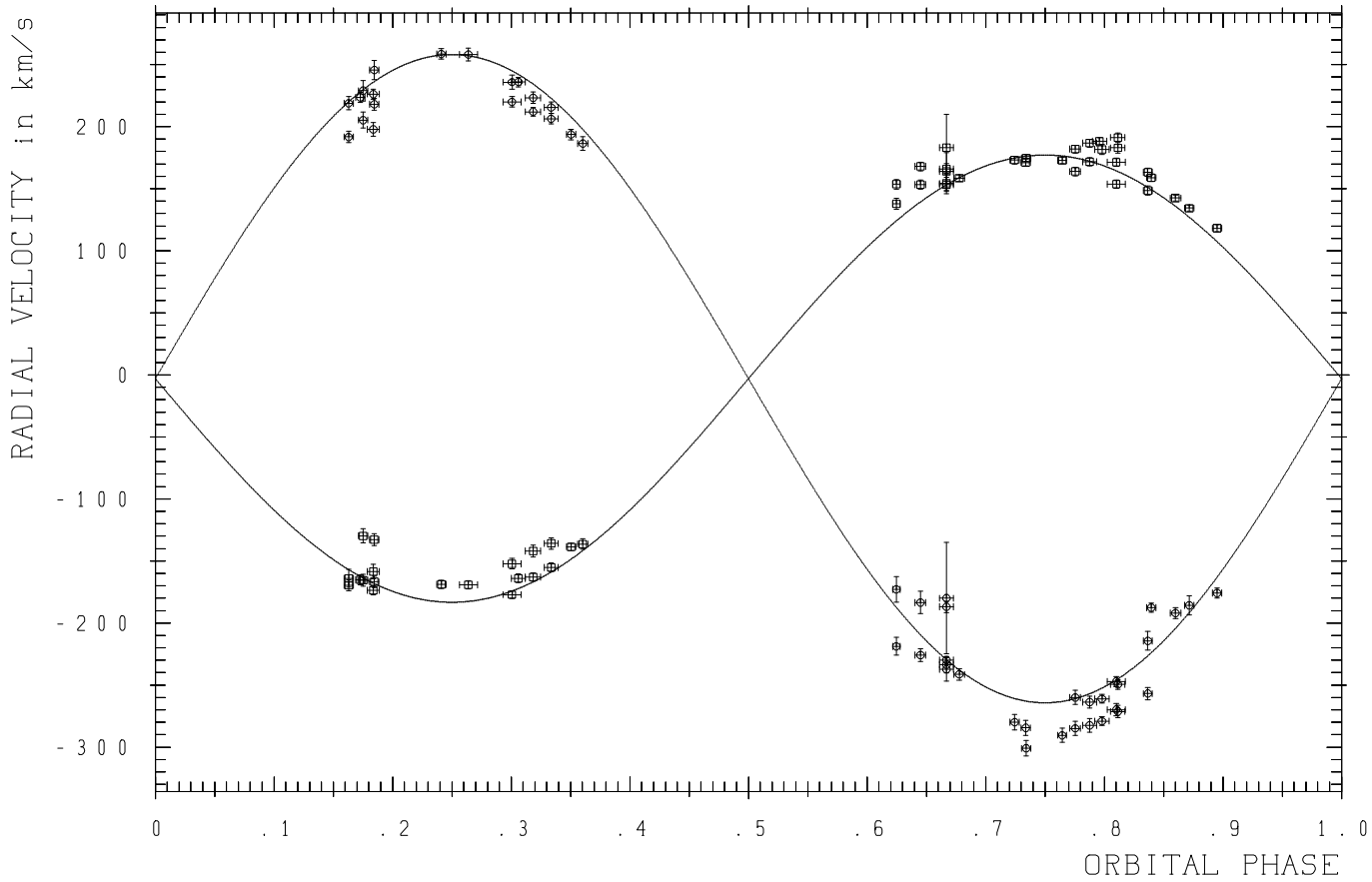

Fig. 3. Radial velocity curves of the eclipsing binary components; observations are shown together with best fit curves.

the third body turned out to be only about 25 km s^{-1}, it was thoroughly checked whether these shifts of the line positions might not be an artifact of the deconvolution method. For this purpose three synthetic Gaussian profiles with FWHMs and central depths similar to those of the observed features were overlayed and folded with different noise functions. To simulate various orbital phases, these features were systematically shifted against each other, with relative wavelength differences of the components' lines similar to those in the real SZ Cam spectra. The artificial blends were then disentangled with the same method like the real features in the observed spectra. The input parameters could be reproduced with high accuracy, except for cases where the wavelength separation of the line components was so small that no unique unfolding of the composite features was possible, or the signal-to-noise ratio was assumed too poor. For example, the deviation of the third line's position from the input value was in the range of 0 to 3 km s^{-1} (for orbital phases at least 0.1 phase units outside of eclipses). Otherwise no systematic effects could be recognized, which could have erroneously produced a radial velocity variation of the third component lines similar to the third body radial velocity curve derived from the observed spectra. As an additional test of our results, the KOREL code (Hadrava 1995) was applied to our data. This is a Fourier transform method for disentangling composite stellar spectra of binary or multiple stars. The decomposition of our spectra with this method also confirmed our results (Drechsel et al. 1997). The *double binarity* of the multiple system ADS 2984 B is further supported by the interferometric results (see Sect. 4).

The comparison of the radial velocity measurements of the third component in different seasons made it possible to confirm their periodicity. The time separation of our different observing runs is however such, that the number of epochs in the gaps between the observing seasons cannot uniquely be determined. Therefore, an aliasing problem exists with the interpretation of the power spectra. The maximum power value corresponds to a period of $2\overset{\mathrm{d}}{.}7966$, but there are more alias peaks in the vicinity of this value, e.g. at $2\overset{\mathrm{d}}{.}7717$ and $2\overset{\mathrm{d}}{.}8233$. As the radial velocity curve derived from the first value gives minimum scatter in a phase-dependent representation of the data, this period was preferred.

Since the zero point in phase for the radial velocity curve of the third body was a priori unknown, an arbitrary reference epoch was chosen, being identical with the exposure of our first SZ Cam spectrum (hel. JD $2448999\overset{\mathrm{d}}{.}3472$). Using $P_{\mathrm{T}} = 2\overset{\mathrm{d}}{.}7966$, relative phase values $\hat{\phi}_{\mathrm{T}}$ for the radial velocities of the third component in our 31 spectra were calculated. Assuming

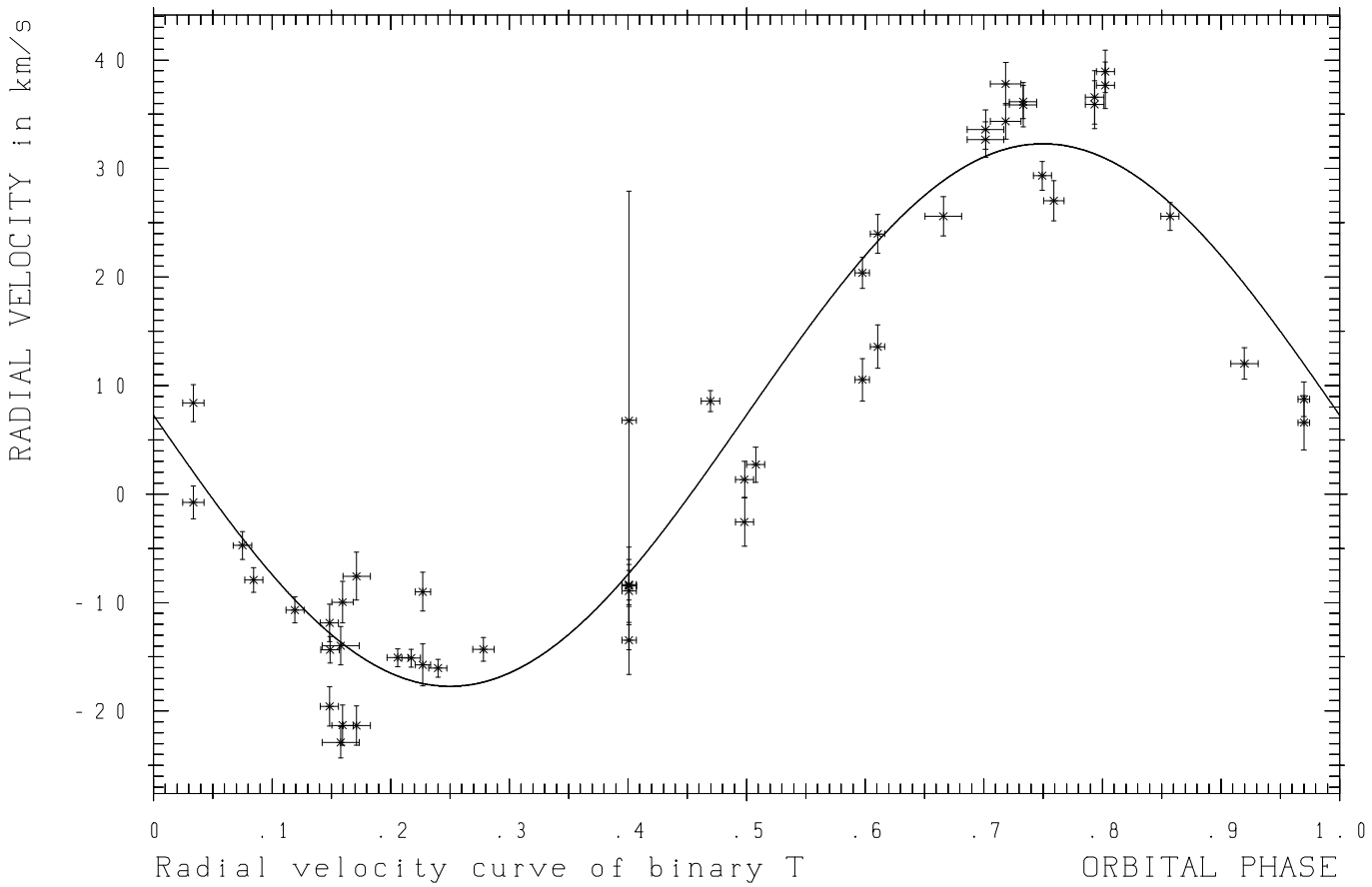

Fig. 4. Radial velocity curves of the third body (binary T); observations are shown together with best fit curves. Phases were calculated using the ephemeris T_0 = hel. JD2448998$^{\rm d}$.0608 + 2$^{\rm d}$.7966 · E.

an orbital eccentricity $e = 0$, the data were then fitted with a sine function of the form

$\gamma_{0,\rm T} + K_{\rm T} \cdot \sin(\hat{\phi}_{\rm T} + \Delta\phi_{\rm T})$,

yielding the following best fit values for the amplitude $K_{\rm T}$, the systemic velocity $\gamma_{0,\rm T}$, and the phase shift $\Delta\phi_{\rm T}$ of binary T:

$\gamma_{0,\rm T}$ = 7.3 km s^{-1} $\pm$ 0.9 km s^{-1},

$K_{\rm T}$ = 25.0 km s^{-1} $\pm$ 1.1 km s^{-1}, and

$\Delta\phi_{\rm T}$ = 2.9505 rad $\equiv$ 0.4697 · $P_{\rm T}$ = 1$^{\rm d}$.31345.

With the phase shift $\Delta\phi_{\rm T}$ known, a new reference epoch and the following ephemeris for binary T can be given:

T_0 = hel. JD 2448998$^{\rm d}$.0608 + 2$^{\rm d}$.7966 · E.

In order to follow the usual convention, the above reference epoch was chosen such that T_0 represents an epoch of spectroscopic conjunction ($\phi_{\rm T} = 0.0$), i.e. the time of minimum radial velocity (at $\phi_{\rm T} = 0.25$ minus $P_{\rm T}/4$). It should be noted that this ephemeris is rather preliminary, and should be improved by future measurements. The radial velocity curve of binary T is shown in Fig. 4.

The small velocity amplitude $K_{\rm T}$ of the third body combined with a large value of its mass function (see below) means that the orbit of this binary T must have a quite different inclination than the eclipsing pair. If we accept the mass sum $m_{1,\rm T} + m_{2,\rm T}$ = 19.7 M$_\odot$ resulting from an analysis of the light time effect (see Paper I and solution 1 of Table 6), and a mass ratio $q_{\rm T} = m_{2,\rm T}/m_{1,\rm T}$ of say 0.5 (i.e. a relatively small value, because the secondary lines are not visible), the masses of the binary T components would amount to $m_{1,\rm T}$ = 13.1 M$_\odot$ and $m_{2,\rm T}$ = 6.6 M$_\odot$. The orbital inclination could then only amount to $i_{\rm T} \approx 20°$. One can of course speculate that the visible third body line is an unresolved blend of primary and secondary components, which would mean that the real $K_{1,\rm T}$ could be larger than determined here, and $q_{\rm T}$ might also be somewhat larger, so that $i_{\rm T}$ would then increase to approximately 30°.

2.5. Determination of equivalent widths

Equivalent widths of lines cannot be determined from binary or multiple star spectra without disentangling the composite continua of the different stars involved. In the case of SZ Cam the

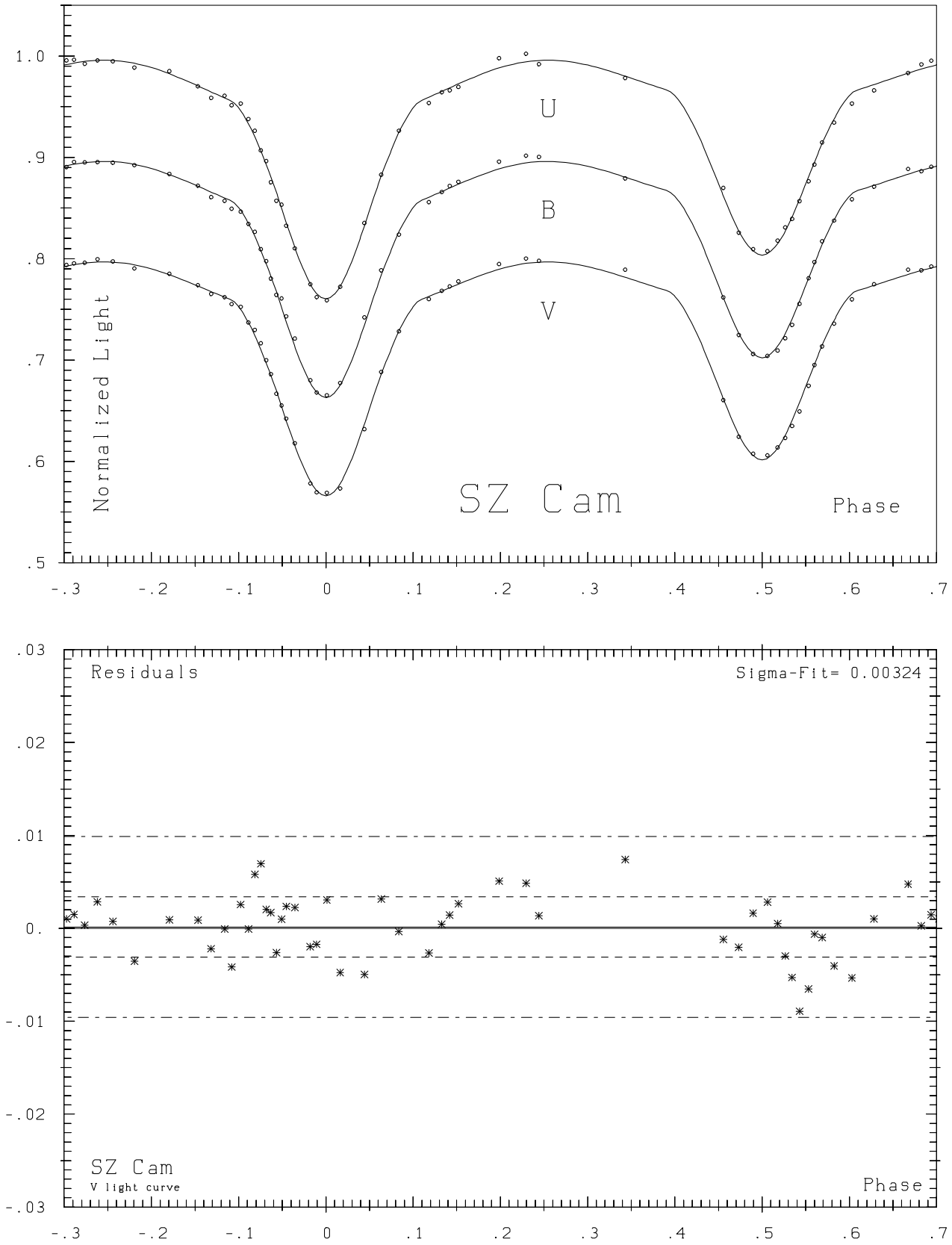

Fig. 5. Top: computed UBV light curves of SZ Cam together with normal points by Kitamura & Yamasaki (1970). Bottom: residuals between the V curve and normal points. The mean residual value is $1.5 \cdot 10^{-4}$, weighted standard deviation is $3.24 \cdot 10^{-3}$; 1σ and 3σ belts are shown as dashed and dash-dotted lines, respectively

Table 3. Equivalent widths (EWs) and FWHMs for some He I lines (in Å); the 3rd, 5th, and 7th columns contain measured EWs with respect to the composite continuum, while the last three columns give true EWs with respect to the relative continuum contributions of the individual stellar components

Line	No. of spectra	Primary		Secondary		Third body		Primary	Secondary	Third body
		EW	FWHM	EW	FWHM	EW	FWHM	true EW	true EW	true EW
He I 4713	1	0.19	3.88	0.05	1.80	0.09	1.52	0.38	0.25	0.28
He I 4922	15	0.41	4.40	0.12	3.40	0.15	1.89	0.83	0.58	0.48
He I 5016	15	0.18	3.71	0.04	2.16	0.09	1.63	0.38	0.17	0.30
He I 6678 [a]	6	0.41	4.78	0.11	4.00	0.21	2.43	0.83	0.53	0.70
He II 4542	1	0.09	3.57	0.01	1.88	0.04	2.30	0.19	0.02	0.12
He II 4686	1	0.24	3.60	0.02	1.14	0.08	1.88	0.49	0.08	0.25
Si III 4553	1	0.13	3.81	0.04	2.12	0.07	1.28	0.27	0.17	0.21
Si III 4568 [b]	1			0.03	2.28	0.07	1.59		0.13	0.21
Si III 4575 [c]	1	0.06	4.26			0.03	1.25	0.13		0.10

[a] For the He I 6678 line, only measurements with phases $\lesssim 0.5$ are used, since at phases > 0.5 the line is strongly blended with other features.
[b] Primary line strongly blended with Si III 4575 secondary line, and therefore not used.
[c] Secondary line strongly blended with Si III 4568 primary line, and therefore not used.

total continuum is composed of the continua of four stars, two of them with unknown effective temperatures. An approximation with Planck functions as it was performed with the spectra of the O-type binary AB Cru (Lorenz et al. 1994) is therefore not recommended here. On the other hand, ratios of equivalent widths of different lines originating from the same stellar component are independent of the continuum level and can be calculated. This is possible at least for the primary and secondary components of SZ Cam, whereas the third line is probably an unresolved blend of the two components of binary T. In Table 3 we give the measured equivalent widths for selected spectral lines.

According to our photometric solution (see Sect. 3), the primary component contributes 0.486, the secondary 0.207 and the tertiary 0.307 to the total light in the visual region (the wavelength dependence is only weak and is neglected here). In the last three columns of Table 3 we give the measured EWs divided by these numbers, i.e. the true EWs for the individual components.

3. Photometric solution

The photoelectric UBV light curves of Kitamura & Yamasaki (1970) were previously solved in several papers, however never with the possibility of non-zero l_3 in mind. We now performed a new solution with our MORO code, which uses the general logistics of the Wilson-Devinney approach (Wilson & Devinney 1971) for the light curve calculation and the SIMPLEX algorithm as parameter optimization method. This program has especially been designed for application to early-type eclipsing binaries, because it also accounts for the influence of radiation pressure exerted via the mutual irradiation of the components of hot, close binary systems (see Drechsel et al. 1995).

The light curve analysis was performed on DEC 3000-300 and 400-4/233 AXP workstations running under the OpenVMS V6.2 operating system. A total of 53 normal points were formed from Kitamura & Yamasaki's (1970) 538 individual measurements in each colour. Four normal points around the center of the primary, six normal points around the center of the secondary minimum, and five normal points around the maximum at $\phi = 0.75$ were weighted five times higher than the rest of the curve, in order to emphasize the importance of these phase ranges for the solution. Typically 200 to 300 iterations, depending on the start values and increments of the adjustable parameters, were necessary to achieve convergent solutions. For the light curve analysis of SZ Cam we used a program mode, which implies no restrictions with respect to the system configuration. In this mode the luminosity L_2 of the secondary component is correlated with its effective temperature T_2 by means of a Planck function. As for the light curve analysis only the ratio $(T_1/T_2)^4$ of the effective temperatures of the stellar components is relevant, the primary effective temperature T_1 was fixed at 33 000 K, which is consistent with Budding's (1975) spectral classification as O9.5 V as well as our preferred type O9 IV (see also Sect. 6).

Generally light curve solutions of early-type eclipsing binaries sensitively depend on the mass ratio q. Therefore, the knowledge of an independently determined value of q, i.e. the use of a spectroscopic mass ratio is a valuable help. In our case, the mass ratio was nevertheless treated as an adjustable parameter with a start value equaling $q_{\rm spec} = 0.69$ and rather small start increments. Actually the photometric value converged very close to the spectroscopic mass ratio, hence confirming its reliability.

As generally assumed for OB-type stars with atmospheres in radiative equilibrium, the gravity darkening coefficients were fixed at $g_1 = g_2 = 1$, and the bolometric albedos at $A_1 = A_2 = 1$; theoretical limb darkening coefficients were taken from Wade & Rucinski (1985) for the corresponding spectral types:

x_1(U) = 0.310, x_2(U) = 0.345;
x_1(B) = 0.300, x_2(B) = 0.340;
x_1(V) = 0.250, x_2(V) = 0.280.

Table 4. Light curve solutions

Parameter	$l_3 \approx 20\,\%$	$l_3 \approx 30\,\%$
T_1 [a]	33 000 K	33 000 K
T_2	28 050 K (±500)	27 450 K (±250)
i	73.°8 (±0.6)	77.°0 (±0.6)
q [b]	0.698 (±0.015)	0.704 (±0.015)
Ω_1 [c]	3.424 (±0.14)	3.405 (±0.06)
Ω_2 [c]	3.510 (±0.04)	3.711 (±0.13)
L_1(U) [d]	0.677 (±0.005)	0.716 (±0.013)
L_2(U) [d]	0.323 (±0.005)	0.284 (±0.013)
l_3(U) [e]	21.1 % (±1.5)	31.0 % (±1.5)
L_1(B) [d]	0.670 (±0.003)	0.709 (±0.012)
L_2(B) [d]	0.330 (±0.003)	0.291 (±0.012)
l_3(B) [e]	20.4 % (±1.0)	31.0 % (±1.5)
L_1(V) [d]	0.665 (±0.003)	0.703 (±0.022)
L_2(V) [d]	0.335 (±0.003)	0.297 (±0.022)
l_3(V) [e]	20.5 % (±1.0)	30.5 % (±1.0)
δ_1 [f]	0.038 (±0.015)	0.026 (±0.012)
δ_2 [f]	0.038 (±0.011)	0.018 (±0.014)
r_1(pole) [g]	0.348 (±0.014)	0.355 (±0.018)
r_1(point) [g]	0.390 (±0.020)	0.409 (±0.030)
r_1(side) [g]	0.362 (±0.017)	0.371 (±0.021)
r_1(back) [g]	0.380 (±0.020)	0.391 (±0.025)
r_2(pole) [g]	0.280 (±0.015)	0.266 (±0.023)
r_2(point) [g]	0.305 (±0.022)	0.287 (±0.034)
r_2(side) [g]	0.289 (±0.017)	0.273 (±0.026)
r_2(back) [g]	0.304 (±0.022)	0.285 (±0.033)
r_1 [h]	0.37 (±0.02)	0.38 (±0.03)
r_2 [h]	0.29 (±0.02)	0.28 (±0.03)

[a] fixed parameter;
[b] photometrically adjusted;
[c] surface potential;
[d] relative luminosities $L_i/L_1 + L_2$;
[e] fraction of third light at maximum;
[f] radiation pressure parameter, see Drechsel et al. 1995;
[g] fractional Roche radii in units of separation of mass centers;
[h] mean fractional Roche radius.

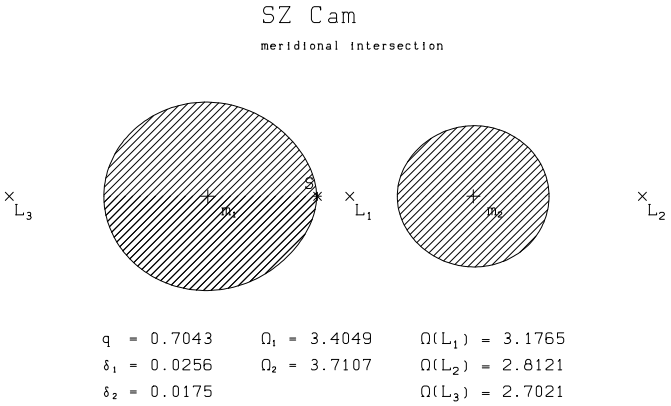

Fig. 6. Meridional intersection of SZ Cam according to the parameters of the light curve solution given in Table 4 ($l_3 \approx 30\,\%$). The mass centers of the primary and secondary components and the systemic center of mass are labeled by m_1, m_2, and S, respectively; the Lagrangean points L_1, L_2 and L_3 are also marked.

Table 5. Absolute dimensions of the SZ Cam eclipsing binary

Primary component		Secondary component	
$M_1/M_\odot$	15.26 ±0.53	$M_2/M_\odot$	10.75 ±0.44
$R_1/R_\odot$ [a]	9.01 ±0.91	$R_2/R_\odot$ [a]	6.63 ±0.68
$L_1/L_\odot$	$8.63 \cdot 10^4$ $\pm 1.76 \cdot 10^4$	$L_2/L_\odot$	$2.25 \cdot 10^4$ $\pm 0.47 \cdot 10^4$
$\log L_1/L_\odot$	4.94 ±0.09	$\log L_2/L_\odot$	4.35 ±0.09
$\log\ T_1$	4.52	$\log\ T_2$	4.44
$\log\ g_1$	3.712	$\log\ g_2$	3.826

[a] radius of sphere with same surface area as distorted star;

Thus, adjustable parameters were the secondary temperature T_2, orbital inclination i, mass ratio q, primary and secondary surface potentials Ω_1 and Ω_2 (yielding their fractional radii), luminosity of primary component L_1 as well as fractional third light l_3 for the U, B, and V ranges, respectively, and radiation pressure parameters of the binary components δ_1 and δ_2, which are defined as the ratio of radiative relative to gravitational forces exerted by the companion on the irradiated surface (see Drechsel et al. 1995).

We obtained several convergent light curve solutions with good fit quality: the weighted standard deviation for the U, B and V curves were typically about 0.0038, 0.0036, and 0.0032 intensity units, respectively. However, we were unable to obtain an unambiguous solution with respect to the amount of third light. Values from about 10 % up to 40 % of the total system luminosity were possible and yielded comparably good overall representations of the observed light curves, as judged from the weighted sums of squared residuals. On the other hand, all convergent light curve solutions yielded non-zero third light, even when the start value of the l_3 parameter was chosen as 0.0. In principle, the true value of l_3 might be deduced from spectral line ratios and also by means of speckle interferometry. The spectral types of all three components do not differ much, nevertheless the ratio of equivalent widths of the lines studied here varies considerably, and hence the accuracy of l_3 obtained by this method is low.

During a survey of duplicity among O stars (Hartkopf et al. 1993), the CHARA group discovered the third body in the SZ Cam system by speckle interferometry. The magnitude difference between the eclipsing pair and the third body was found to be less than about 1.5 mag in the Strömgren y filter passband (Mason 1995), which corresponds to a lower limit of the third light contribution l_3 of 25 % in the visual range. In Table 4, so-

Table 6. Orbital parameters of the eclipsing pair and the third body

Parameter	Solution 1	Solution 2
Long period	50.7 yr	61.0 yr
semi-amplitude A	$0\overset{d}{.}086$	$0\overset{d}{.}096$
eccentricity e	0.77	0.83
length of periastron ω	$23\overset{\circ}{.}7$	$19\overset{\circ}{.}0$
time of periastron	JD 2444340	JD 2444200
$a_{12} \sin i$	21.1 AU	26.8 AU
$f(M_3)$	3.64 $M_\odot$	5.19 $M_\odot$
short period	$2\overset{d}{.}6984708$	$2\overset{d}{.}6984628$
hel. JD_0	$2427533\overset{d}{.}441$	$2427533\overset{d}{.}486$
K_{12}	19.4 km s^{-1}	23.5 km s^{-1}
$i = 90°$:		
M_3	19.7 $M_\odot$	23.3 $M_\odot$
$M_3/(M_1 + M_2)$	0.76	0.89
ρ [a]	74.5 AU	82.7 AU
$(\gamma_0 - \gamma_{0,T})$ [b]	-13.1 km s^{-1}	-10.7 km s^{-1}
$i = 60°$:		
M_3	24.2 $M_\odot$	28.9 $M_\odot$
$M_3/(M_1 + M_2)$	0.93	1.11
ρ [a]	77.2 AU	87.5 AU
$(\gamma_0 - \gamma_{0,T})$ [b]	-11.7 km s^{-1}	-9.6 km s^{-1}

[a] separation of eclipsing pair and third body on JD 2 449 610;
[b] on JD 2 449 400.

lutions with $l_3 \approx 20\,\%$ and $l_3 \approx 30\,\%$ are listed. The given error limits represent intervals of the adjusted parameter values as achieved from various convergent fits with similar fit quality. In the solution with $l_3 \approx 30\,\%$, the amount of third light is best compatible with the value suggested by the speckle interferometric measurement, and the corresponding parameters will be further used here. The best fit for the UBV light curves with $l_3 \approx 30\,\%$, and the corresponding residuals of the V curve are presented in Fig. 5. It should be noted that all more recently published solutions rendered a semi-detached configuration of SZ Cam, whereas any of our new solutions with non-zero l_3 are only in accordance with a detached system configuration.

For the determination of the absolute stellar parameters of the SZ Cam eclipsing binary, the radial velocity amplitudes K_1 and K_2, the orbital inclination $i = 77\overset{\circ}{.}0$, and the photometric mass ratio $q = 0.704$, as derived from the light curve analysis were used. It should be noted that the photometric mass ratios q (taken from solutions with $l_3 \approx 20\%$ as well as $l_3 \approx 30\%$) turned out to lie within the error limits of the spectroscopic value $q_{\rm spec}$. The luminosities were calculated with the adopted effective temperature $T_1 = 33\,000$ K (corresponding to spectral type O9 IV) and $T_2 = 27\,450$ K from the light curve solution. The absolute parameters of the components of the eclipsing system are listed in Table 5. Fig. 6 shows a meridional intersection of the SZ Cam eclipsing pair, and Fig. 7 presents a 3D simulation, based on the light curve solution with $l_3 \approx 30\%$, displaying the system at various orbital phases.

4. The orbit of the third body

In Paper I, the orbital period and other parameters of the third body orbit were derived by an analysis of the light time effect. The $O-C$ curve was however only poorly covered by minimum times, so that the period of 50.7 years given there was not well established. Though this value corresponds to the solution with the smallest $\sum(O-C)^2$, other period values cannot be excluded. A value of 50.7 years is the shortest one, which gives a good representation of the observed times of minima. Yet somewhat longer periods are also acceptable at the expense of only slightly worse fit quality. As an example, an alternate value of 61.0 years has been considered here (it will be shown that still longer periods are not realistic, because they would imply a too large third body mass). The $O-C$ diagram with the theoretical light time curves for both periods is plotted in Fig. 8 together with the observed minimum times; the determined parameters of the third body orbit for the two solutions are contained in Table 6.

The CHARA group measured the companion separated by $0\overset{''}{.}071$ from the eclipsing system at a position angle of $300\overset{\circ}{.}0$ on JD 2 449 610 (Mason 1995). It is of interest to compare this observed value of separation with a value, which follows from our parameters of the third-body orbit. The semi-major axis of the orbit of the eclipsing system around the common center of mass is (see, e.g., Mayer 1990)

$$a_{12} = \frac{173.14\ A}{\sin i \sqrt{1 - e^2 \cos^2 \omega}} \quad \text{(AU)},$$

where $A = \frac{1}{2}[(O-C)_{\max} - (O-C)_{\min}]$ denotes the observed semi-amplitude of the light time curve (in days), i is the inclination of the third body orbit, and ω the length of periastron. The semi-major axis of the relative orbit of the eclipsing pair and the third body is

$$a = a_{12} + a_3 = a_{12} \frac{q_3 + 1}{q_3},$$

where $q_3 = \frac{M_3}{M_1 + M_2}$.

M_3 and i are connected by the mass function

$$f(M_3) = \frac{(M_3 \sin i)^3}{(M_1 + M_2 + M_3)^2}.$$

The observable separation in AU should be (see, e.g., Aitken 1935)

$$\rho = r \frac{\cos(\nu + \omega)}{\cos(\alpha - \Omega)},$$

where

$$r = a \frac{1 - e^2}{1 + e \cos \nu}$$

and

$$\tan(\alpha - \Omega) = \tan(\nu + \omega) \cos i.$$

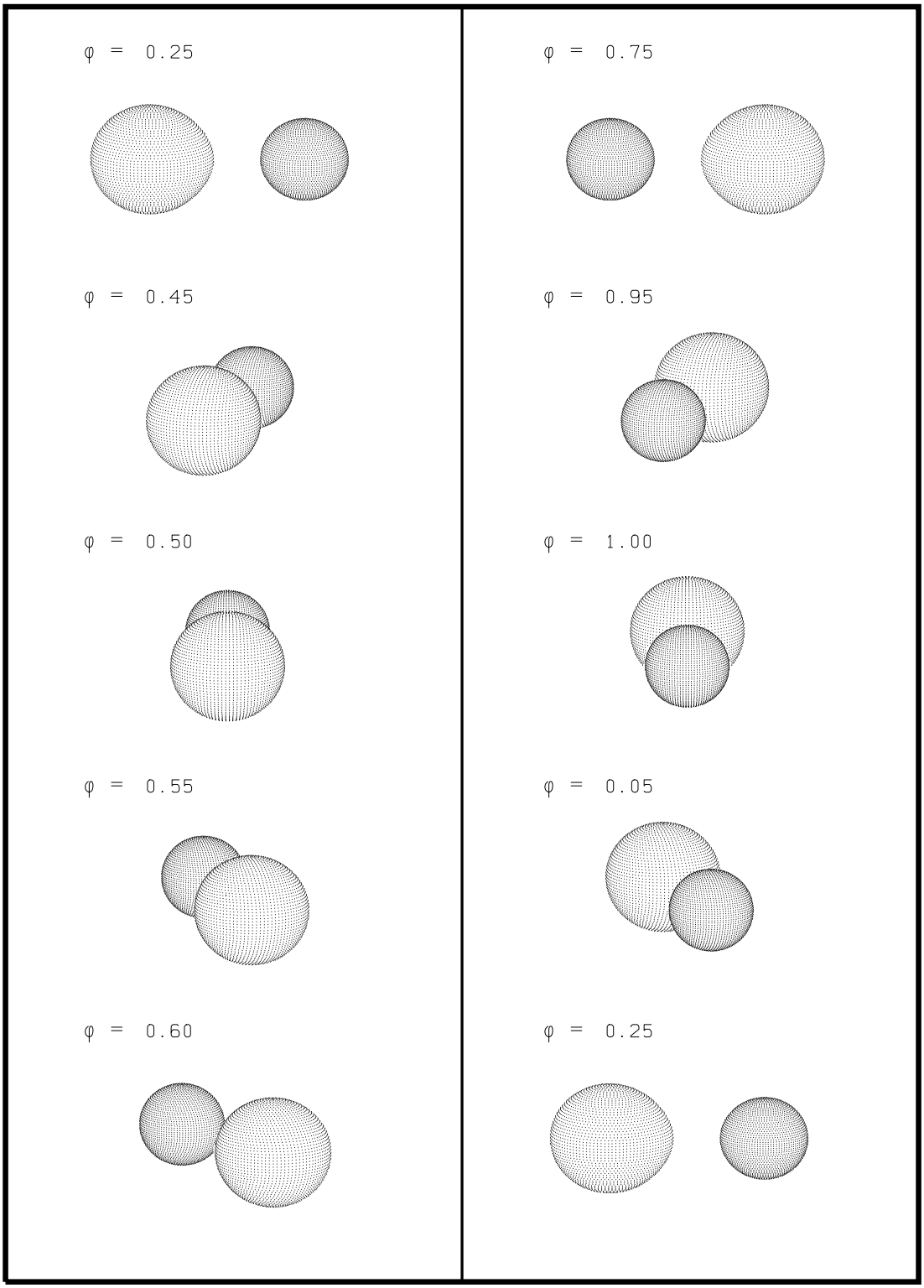

Fig. 7. The SZ Cam "Roche movie": a 3D simulation of the SZ Cam eclipsing pair shown at various orbital phases, based on the results of the light curve solution with $l_3 \approx 30\%$ given in Table 4.

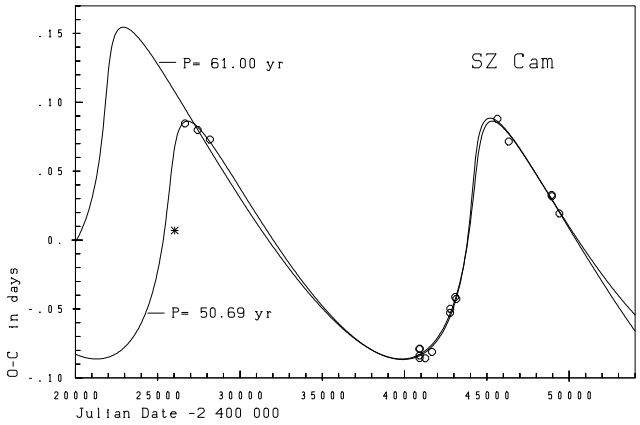

Fig. 8. Fitted light time curves of SZ Cam for two different orbital periods of the third component: 50.7 years and 61.0 years; observed times of minima are shown as circles and were taken from Mayer (1987) and Paper I; one minimum time given by Guthnick & Prager (1930) is marked by "$*$", but was not used due to its unknown accuracy; ephemeris for calculation of $O-C$ values: hel. JD 2 427 533.$^{\rm d}$4412 + 2.$^{\rm d}$6984708 · E.

α and Ω are the position angles of the companion and of the visual orbit nodal line, respectively, and ν is the true anomaly. The separation in seconds of arc is given by $\frac{\varrho}{d}$, where d is the distance of the system from the Sun in parsec. For both periods considered here the linear separation for two assumed values of i (60° and 90°) is found in Table 6. This separation is given for the time of the speckle measurement (1994.7035), and the eclipsing binary mass $M_1 + M_2 = 26.0\,\mathrm{M}_\odot$ (see Sect. 3) has been assumed. The expected visual orbits are presented in Fig. 9.

The large value of the minimum mass of the third body is not easy to satisfy, even so with a confirmed binary nature of this object. The third-body mass increases with increasing third body period and decreasing inclination; therefore, one is inclined to prefer the shortest possible period (50.7 years) and the largest inclination (90°). Then, however, the distance of the system from the Sun would have to be larger than the value of 875 pc determined for the open cluster NGC 1502 with photometric means by Crawford (1994). For a period of 50.7 years and an inclination of 90°, the distance d should be

$$d = \frac{74.5\ \mathrm{AU}}{0.''071} = 1050\ \mathrm{pc}.$$

In Table 6, also calculated differences of the systemic velocities of both binaries for the two different long period values (50.7 and 61.0 yr) and for two arbitrary inclination angles (60° and 90°) are given. The observed value of $\gamma_0 - \gamma_{0,\mathrm{T}} = -10.2$ km s^{-1} lends some support for the longer period and smaller inclination, though the accuracy of this quantity is rather low.

Using Fig. 9 it is possible to forecast the angular separation for the near future: until JD 2 451 000 (mid-1998), it should increase by about 1 milliarcsecond per year, with the position angle changing by no more than about 0.°5 per year.

Unfortunately, it will not be possible to find a more precise value of the long period by timing of minima before about the year 2020. Continued interferometry might however yield the time of apastron, and thereby help constrain the correct value already sooner; of course, it could also provide the important value of the inclination.

Table 7. Radial velocities of the visual companion ADS 2984 A

hel. JD -2440000	Average rv (km s^{-1})	$\delta(rv)$ (km s^{-1})	Number of measurements
8999.6270	-33.1	16.8	2
9001.4929	-52.0	10.2	3
9002.5380	-47.2	9.0	2
9325.5946	+33.1	19.3	2
9328.6335	+22.3	16.2	2
9328.6967	+33.6	5.9	3
9329.4224	+21.6	6.8	3
9329.5043	+23.5	8.5	2
9330.5321	+15.4	7.2	2
9907.6650	+0.1	7.1	3
9913.5798	-29.5	14.7	6
9914.6646	-31.8	8.8	3
9915.5341	-44.2	10.3	3

5. The visual companion ADS 2984 A

The spectral type of ADS 2984 A was given as B0 III by Slettebak (1963) and as B0 II by Abt (1981). However, due to the earlier possible mis-identification of the two visual components of ADS 2984, the Abt classification of B0 IIn of ADS 2984 B might be appropriate for this star. Radial velocity variations of ADS 2984 A based on photographic spectra taken with the 1.8 m telescope of the Dominion Astrophysical Observatory, Victoria (Canada) were reported by Plaskett (1924). He published eight velocity measurements, ranging between -62.6 and +38.8 km s^{-1}. In order to check these old photographic measurements, we took 14 high resolution CCD spectra of ADS 2984 A with the 2.2m telescope of the DSAZ Calar Alto Observatory and the same equipment and instrumental setup as for the SZ Cam spectra. The helium lines He I 4922, 5016, and 6678, Hα and Hβ, and in one case also He I 4713, He II 4542, and 4686 as well as Si III 4553, 4568, and 4575 were used for radial velocity determinations. Since no secondary lines could be detected, the line fits were performed using single Gaussian functions in the same way as described in Sect. 2.2. Table 7 lists the average radial velocities for all evaluated lines in each of our spectra; the standard deviation $\delta(rv)$ is also given there.

The radial velocities vary between -52.0 and +33.6 km s^{-1}, in agreement with Plaskett's (1924) earlier measurements. The time separation of our observing epochs is too large for an unambiguous period determination of the ADS 2984 A binary. The power spectra based on all available velocity data show no reliable signatures of the orbital period; however, an inspection of radial velocities obtained during single observing runs would suggest an orbital period of tens of days.

Fig. 10 presents two typical spectra of ADS 2984 A, taken at hel. JD 2449328.$^{\rm d}$6967 and 2449330.$^{\rm d}$5321 in the spectral ranges of the Hβ and Hα lines, respectively. FWHMs are given

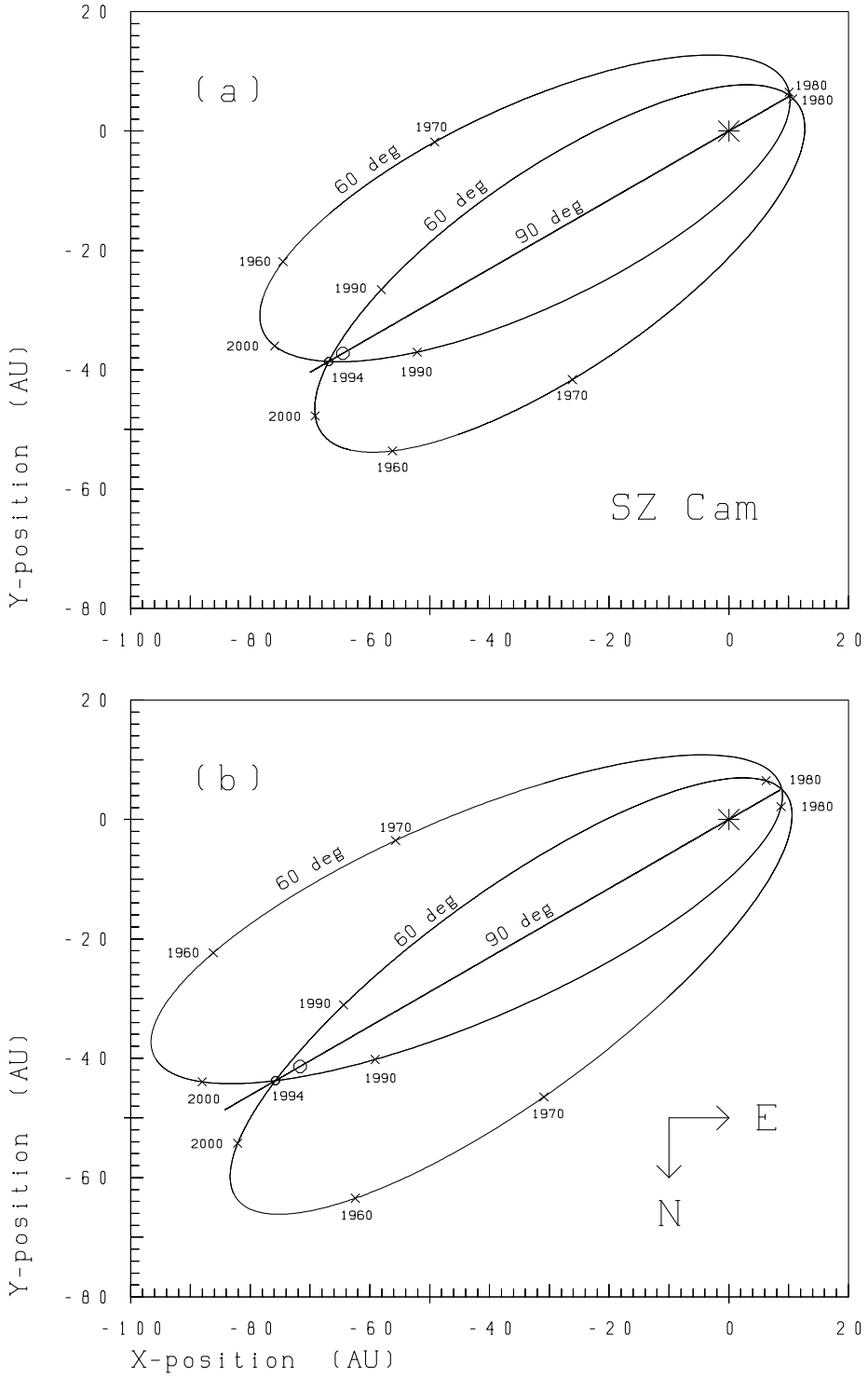

Fig. 9a and b. Visual orbits of the third component projected on the celestial sphere for orbital periods of 50.7 (**a**) and 61.0 years (**b**).

in Table 8. It is evident that the line profiles are significantly broader than those of the SZ Cam components. The FWHMs of the He I lines lie within the range of 5.42 to 7.95 Å, those of the He II and Si III lines are slightly smaller. In order to check whether the broadened profiles represent unresolved blends of primary and secondary lines, our measurements were tested for possible correlations between FWHMs and radial velocities (as derived from the Gaussian fits), and on the other hand between FWHMs and absorption depths. If the observed line profiles were due to such blends, the FWHMs of the unresolved features should vary with orbital phase: e.g., at orbital phase 0.0, a maximum absorption depth and a minimum FWHM of the unresolved profile should be expected. However, no significant correlations of this kind are apparent. Therefore, the broad line profiles are very likely due to the fast rotation of the primary component of ADS 2984 A, which certainly dominates

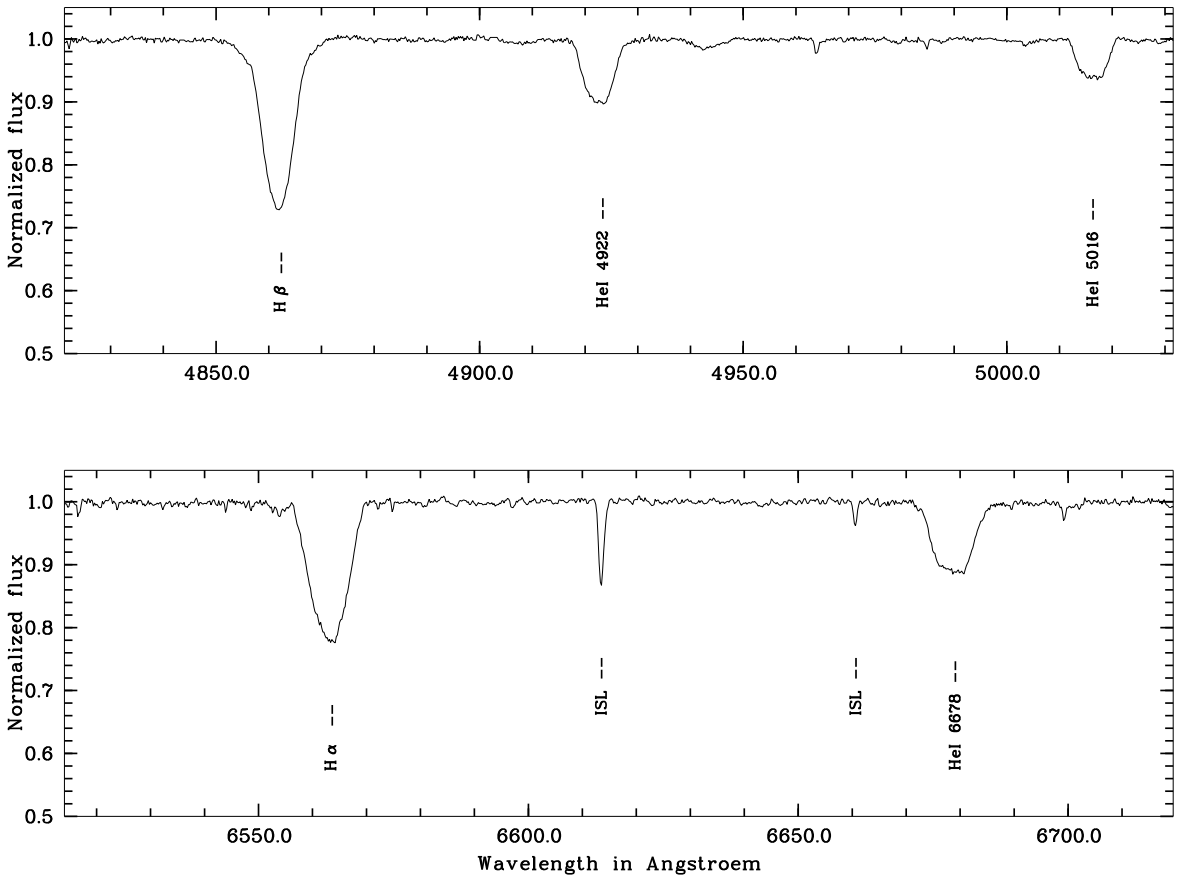

Fig. 10. Typical spectra of ADS 2984 A obtained with the Coudé spectrograph at the 2.2m telescope of Calar Alto Observatory. The spectra were taken at hel. JD 2449328$^{\rm d}$.6967 (top) and 2449330$^{\rm d}$.5321 (bottom)

the spectrum of this binary. This is also supported by the sharp transition between the continuum and the absorption wings of helium and silicon lines, which is a typical signature of fast rotating stars with a small degree of limb darkening. The line widths correspond to $v \sin i \approx 220 \pm 20$ km s^{-1}, which is not unusual for early B-type stars. In a close binary, the rotation should be synchronized with the orbital period on a relatively short timescale of about 10^5 years (Tassoul & Tassoul 1992), depending on the radii and separation of the involved stars. The synchronization time will, however, be one order of magnitude longer for a binary with an orbital period of several tens of days, which is probably the case for ADS 2984 A. Hence it appears not unlikely that this star is still being observed in a non-synchronous rotation phase.

Table 8 also gives observed and calculated equivalent widths for ADS 2984 A. Since in our spectra no secondary lines are visible, the contribution of the secondary component to the total flux can be estimated to be less than about 5 %, and hence the equivalent widths can essentially be attributed to the primary component of the visual companion. For comparison, also ratios of equivalent widths of the ADS 2984 A primary relative to the SZ Cam primary and secondary components are included in Table 8.

The equivalent widths of the He I lines of ADS 2984 A are fairly similar to those of the SZ Cam primary, but about twice as strong compared with the secondary component. Since the SZ Cam primary exhibits a clear helium over-abundance (see Sect. 6.2), the similarity with respect to the equivalent widths of the He I lines of both stars suggests a helium over-abundance of ADS 2984 A, too. On the other hand, the He II lines 4542 and 4686, which are very sensitive to the effective temperature, are about a factor of 2 weaker than those of the SZ Cam primary, but more than twice as strong as those of the SZ Cam secondary. It is therefore suggested that the ADS 2984 A primary component might be of slightly later spectral type than the SZ Cam primary ($T_{\rm eff}$ = 33 000 K). However, it should be significantly hotter than the SZ Cam secondary, which has an effective temperature of about 27 500 K, equivalent to spectral type B0.5 V (see Table 4).

This is also supported by a comparison between the observed and calculated equivalent widths of ADS 2984 A, for which a giant log g value of 3.5 was assumed (for details see Sect. 6.2). At solar He abundance (0.1), the observed equivalent widths of the He I lines are about a factor of 2 stronger than the calculated ones, and those of the He II lines fit the observations better at $T_{\rm eff}$ = 31 000 K than at 30 000 K. The situation

Table 8. FWHMs and equivalent widths (EWs) of ADS 2984 A lines. Ratios between the values for the primary component of the visual companion (SB1 binary "ADS") and the primary and secondary components of SZ Cam ("SZ1" and "SZ2", respectively) are also given.

Line	observed FWHM (Å)			observed EW (Å)			calculated [a] EW (Å) for			
	ADS	ADS/SZ1	ADS/SZ2	ADS	ADS/SZ1 [b]	ADS/SZ2 [c]	n(He) = 0.1		n(He) = 0.3	
							30000 K	31000 K	30000 K	31000 K
He I 4713	6.02	1.55	3.34	0.43	1.10	1.79	0.20	0.16	0.25	0.25
He I 4922	5.87	1.33	1.73	0.69	0.82	1.19	0.47	0.44	0.73	0.71
He I 5016	5.42	1.46	2.51	0.39	1.05	2.05	0.20	0.20	0.24	0.24
He I 6678	7.95	1.66	1.99	0.98	1.16	1.85	0.53	0.54	0.63	0.79
He II 4542	3.81:	1.07:	2.03:	0.11:	0.59:	2.20:	0.14	0.24	0.20	0.30
He II 4686	4.61	1.28	4.04	0.27	0.55	2.70	0.12	0.27	0.26	0.36
Si III 4553	5.40	1.42	2.55	0.30	1.12	1.58				
Si III 4568	5.32		2.33	0.22		1.57				
Si III 4575	4.77	1.12		0.11	0.89					

[a] according to Napiwotzki (1997); assumed log g = 3.50; for details see Sect. 6.2;
[b] for a contribution of the primary to the composite continuum of the SZ Cam system of 48.6 % as calculated from the light curve solution with $l_3 \approx 30\%$;
[c] for a contribution of the SZ Cam secondary of 20.7 %.

is different, if a He abundance of 0.3 at $T_{\rm eff}$ = 30 000 K is considered. The calculated equivalent widths of the He I lines then closely match the observed values, and those of the He II lines fit the observed quantities perfectly (4686) or at least fairly well (4542). Increasing the temperature to 31 000 K has not much effect on the He I line strengths, whereas the He II lines become considerably too strong. At still higher effective temperatures, the equivalent widths of the He II lines still increase, whereas at $T_{\rm eff} < 30\,000$ K they become too small, even if a He abundance as high as 1.0 is considered. Therefore, n(He) $\approx$ 0.3 or slightly higher, and an effective temperature of about 30 000 K is suggested for the primary component of ADS 2984 A. This is compatible with the spectral classification of the visual companion by Slettebak (1963) and Abt (1981).

6. Discussion and conclusions

6.1. Distance modulus

Using the results of our light curve solution, the photometric distance of the SZ Cam system can be calculated. With the interstellar absorption $A_V = 2\overset{\rm m}{.}32$ derived by Crawford (1994) for the open cluster NGC 1502, the total visual magnitude corrected for interstellar extinction is

$$V_0 = m_V - A_V = 6\overset{\rm m}{.}92 - 2\overset{\rm m}{.}32 = 4\overset{\rm m}{.}60.$$

The light curve solution with $l_3 \approx 30$ % (see Table 4) yields the contribution of each stellar component to the total flux. At orbital phase 0.25 (i.e. outside of eclipse) these are: 48.6 %, 20.7 %, and 30.7 % for the primary, secondary, and third component (binary T), respectively. Thus, the visual magnitudes corrected for interstellar absorption are:

$$V_0(1) = 5.38, \quad V_0(2) = 6.31, \quad \text{and} \quad V_0(3) = 5.88$$

for the three stellar components. With the absolute bolometric magnitude of the Sun, $M_{\rm bol}$(Sun) = 4.75, and the luminosities taken from Table 5, the absolute bolometric magnitudes of the SZ Cam primary and secondary are $M_{\rm bol}(1) = -7\overset{\rm m}{.}60$ and $M_{\rm bol}(2) = -6\overset{\rm m}{.}13$, respectively. Since the absolute dimensions suggest a slightly evolved state of the primary, the following bolometric corrections for luminosity class IV interpolated from Schmidt-Kaler's (1982) tables for 33 000 and 27 500 K, respectively, were used: B.C.(1) = -3 $\overset{\rm m}{.}$28 and B.C.(2) = -2 $\overset{\rm m}{.}$83. The resulting absolute visual magnitudes and distance moduli then are:

$$M_V(1) = -4\overset{\rm m}{.}32, \quad (m_V - M_V)_1 = 9.70, \quad d = 871 \text{ pc}$$
$$M_V(2) = -3\overset{\rm m}{.}30, \quad (m_V - M_V)_2 = 9.61, \quad d = 836 \text{ pc}.$$

The small difference between the distances derived from the primary and secondary is possibly due to the uncertainty in the bolometric correction. The distance moduli agree very well with the value for the open cluster NGC 1502 of $9\overset{\rm m}{.}71$ determined by Crawford (1994) by photometric means.

The interpretation of the interferometry as discussed in Sect. 4 suggests a somewhat larger distance of 1050 pc (distance modulus 10.11 mag), but still within Crawford's error limit, if his standard deviation of $0\overset{\rm m}{.}42$ is considered. However, such increased distance would also imply higher absolute magnitudes; a distance modulus of 10.11 mag would correspond to an effective temperature of about 35 000 K.

The parallax of SZ Cam given in the HIPPARCHOS catalog could not be used, because its error seems too large, and is probably inapplicable in any case due to the unresolved multiplicity of the system.

6.2. Temperatures, equivalent widths, and helium abundance

As shown above, T_1 = 33 000 K corresponding to spectral type O9 IV reasonably agrees with the distance of SZ Cam. This effective temperature is compatible with physical parameters for O stars, published by Howarth & Prinja (1989), too, who give

Table 9. Calculated and observed equivalent widths (Å) for the components of the eclipsing binary

Line	Primary [a]					Secondary [b]				
		calc. EW for			obs. EW		calc. EW for			obs. EW
	n(He) =	0.1	0.3	1.0		n(He) =	0.1	0.3	1.0	
He II 4542		0.37	0.48	0.71	0.19:		0.02	0.04	0.11	0.02:
He II 4686		0.45	0.56	0.78	0.49		0.07	0.10	0.19	0.08
He I 4713		0.20	0.26	0.32	0.38:		0.22	0.28	0.35	0.25:
He I 4922		0.46	0.75	1.09	0.83		0.62	0.94	1.32	0.58
He I 5016		0.20	0.25	0.32	0.38		0.22	0.28	0.37	0.17
He I 6678		0.56	0.73	0.94	0.83		0.50	0.63	0.80	0.53

[a] $\log g = 3.71$; $T_{\rm eff} = 33\,000$ K
[b] $\log g = 3.83$; $T_{\rm eff} = 27\,450$ K

$T_{\rm eff}$ = 34 000 K and $T_{\rm eff}$ = 32 500 K for spectral types O9 V and O9 III, respectively. Also, T_2 = 27 500, following from the light curve solution, leads to a well compatible distance modulus. Moreover, a consideration of equivalent widths can independently be used to verify the derived effective temperatures. The measured equivalent widths of the SZ Cam eclipsing components were therefore compared with calculations by Napiwotzki (1997). For this purpose a code developed by Werner (1986) was applied, assuming plane-parallel non-LTE model atmospheres in radiative and hydrostatic equilibrium and making use of model atoms described in Napiwotzki & Rauch (1994). A grid of equivalent widths of various He I, He II, and H lines was computed for different temperatures, $\log g$ values, and helium abundances. These data were interpolated for the effective temperatures and $\log g$ values of the binary components determined by our photometric solution (see Table 5) for three different He abundances 0.1 (solar), 0.3, and 1.0 (by number). Observed and calculated equivalent widths are compared in Table 9.

For the secondary component the observed equivalent widths are obviously in very good agreement with a solar helium abundance of n(He)/n(H) = 0.1, while it is evident that the primary is definitely He-overabundant. This can mainly be concluded from a comparison of the most reliable line strengths of the He I lines 4922, 5016, and 6678 with the calculated grid values, which suggest a helium abundance in the range of about 0.4 - 0.8. The observed widths of He II 4542 and He I 4713 are less certain, because these could be measured in one spectrum only; nevertheless the latter line also indicates a helium overabundance of the primary. Evolutionary calculations for massive stars (e.g. by Schaller et al. 1992) have shown that such helium enrichment can be the result of the strong stellar wind of a massive O star.

It should also be noted that the simultaneous good agreement of the primary and secondary equivalent widths with theoretical values yield clear support for the effective temperatures and absolute dimensions of the SZ Cam eclipsing pair components as a result of the light curve analysis.

6.3. Evolutionary state

In order to determine the evolutionary state of SZ Cam, the absolute stellar quantities as given in Table 5 were first compared with theoretical predictions for single stars. For spectral type O9 V ($\log T_{\rm eff}$ = 4.52), according to Harmanec (1988) a mass of 16 $M_\odot$ and a radius of 6.2 $R_\odot$ should be expected. For spectral type B0.5 V ($\log T_{\rm eff}$ = 4.45), the values are 12 $M_\odot$ and 6.1 $R_\odot$, respectively. Therefore the radius of the primary component is nearly 50 % larger than that of a single main sequence star of similar mass, and a slightly evolved spectral type of O9 IV has to be preferred. Though the secondary parameters more closely match those of a main sequence star of type B0.5 V, there is still a discrepancy for its mass, which is about 10 % too small.

The derived absolute dimensions of SZ Cam were also compared with evolutionary grids for single stars by Maeder & Meynet (1988) and Schaller et al. (1992), taking into account stellar wind mass loss and convective core overshooting. Evolutionary tracks for solar abundances (Z = 0.02) as well as for higher metallicity (Z = 0.04) were compared with our data. No simultaneous match for all relevant parameters (mass, effective temperature, luminosity) could be found. For example, an initial mass of 40 $M_\odot$ yields an actual mass of 15.31 $M_\odot$ (comparable to M_1) after $5.24 \cdot 10^6$ years, but the corresponding effective temperature and luminosity of the SZ Cam primary are then considerably higher than observed ($\log T$ = 5.14 versus 4.52, and $\log L_1/L_\odot$ = 5.59 versus 4.94 for the theoretical and observed values, respectively). On the other hand, with an initial mass of 20 $M_\odot$, the grid yields M = 15.11 $M_\odot$ after $9.9 \cdot 10^6$ years, but a too low temperature ($\log T_1$ = 3.60) and a too high luminosity ($\log L/L_\odot$ = 5.27), i.e. such star would already be too much evolved to fit the actual physical properties of the primary. No reasonable match with the observed parameters could be obtained by trying a variety of other primary start masses. Hence, an interaction-free evolution according to a single star scheme can be excluded for the SZ Cam eclipsing pair.

We therefore used evolutionary sequences for binary stars by de Loore & De Greve (1992), which account for case B mass transfer (i.e. mass transfer after core hydrogen exhaustion), convective core overshooting and stellar wind mass loss, for comparison with the deduced stellar quantities. However, no coincidence could be found within the parameter range covered by these published evolutionary grids. Especially the actual orbital period of $2\overset{\rm d}{.}69$ is much shorter than any of the theoretical periods resulting from the numerical calculations of de Loore & De

Greve (1992). This might possibly be due to the range of initial periods selected by these authors. Since both components are still close to the main sequence, and the orbital period is rather short, case A evolution is a more probable alternative.

From a comparison of the actual absolute dimensions with Sybesma's (1985; 1986) case A calculations we could find no reasonable match either, the main discrepancies being the observed over-luminosity of the mass gainer for its given mass, and its helium enrichment. Perhaps different starting parameters, i.e. a small initial mass ratio or non-conservative mass exchange, could lead to a better agreement. However, for the time being, the evolutionary state of SZ Cam remains of speculative nature.

Acknowledgements. We thank Dr. B.D. Mason for providing unpublished speckle interferometric results and valuable suggestions. Dr. R. Napiwotzki kindly carried out model atmosphere calculations for the determination of equivalent widths. This work was supported in part by the *Deutsche Forschungsgemeinschaft, DFG* grants Dr 131/8-2,3 and 436 CSR 113/39/1. The assistance of the staff of the *Calar Alto Observatory* is gratefully acknowledged.

References

Abt H.A. 1981, ApJS 45, 437
Aitken R.G. 1935, The Binary Stars, p.79, McGraw-Hill, New York & London
Budding E. 1975, Ap&SS 36, 329
Chochol D. 1977, IBVS 1237
Chochol D. 1980, BAC 31, 321
Crawford D.L. 1994, PASP 106, 397
de Loore C. & De Greve J.P. 1992, A&AS 94, 453
Delgado A.J. 1993, private communication
Drechsel H., Haas S., Lorenz R., Gayler S. 1995, A&A 294, 723
Drechsel H., Weeber, M., Lorenz R., Hadrava, P. 1997, Astron. Ges. Abstr. Ser. 13, 207
Guthnick P., Prager R. 1930, Astron. Nachr. 239, 14
Hadrava P. 1995, A&AS 114, 393
Harmanec, P. 1988, Bull. Astron. Inst. Czech. 39, 329
Hartkopf W.I., Gies D.R., Mason B.D., Bagnuolo W.G., McAlister H.A. 1993, BAAS 25, 872
Howarth I.D., Prinja R.K. 1989, ApJS 69, 527
Irsmambetova T.R. 1994, private communication
Kitamura M., Yamasaki A. 1970, Bull. Tokyo 0bs. No. 220
Lorenz R., Mayer P., Drechsel H. 1994, A&A 291, 185
Maeder A., Meynet G. 1988, A&AS 76, 411
Mason B.D. 1994, Annual Report *Canada-France-Hawaii Telescope Corporation*, p.31
Mason B.D. 1995, private communication
Mayer P. 1987, BAC 38, 58
Mayer P. 1990, BAC 41, 231
Mayer P., Hadrava P., Harmanec P., Chochol D. 1991, BAC 42, 230
Mayer P., Lorenz R., Chochol D., Irsmambetova T.R. 1994, A&A 288, L13 (Paper I)
Mayer P., Lorenz R., Drechsel H. 1997, A&A 320, 107
Morgan W.W., Code A.D., Whitford A.E. 1955, ApJS 2, 41
Napiwotzki R. 1997, private communication
Napiwotzki R., Rauch T. 1994, A&A 285, 603
Plaskett H.H. 1924, Publ. Dominion Astrophys. Obs. Victoria 2, 304
Polushina T.S., Pustylnik I.B. 1994, Astr. Astrophys. Trans. 5, 303
Schaller G., Schaerer D., Meynet G., Maeder A. 1992, A&AS 96, 269
Schmidt-Kaler Th. 1982, in Landolt-Börnstein Vol. 2b, Springer- Verlag Berlin, Heidelberg, New York, p. 453
Slettebak A. 1963, ApJ 138, 118
Sybesma C.H.B. 1985, A&A 142, 171
Sybesma C.H.B. 1986, A&A 159, 116
Tassoul J.-L., Tassoul M. 1992, ApJ 395, 259
Wade R.A., Rucinski S.M. 1985, A&AS 60, 471
Werner K. 1986 A&A 161, 177
Wesselink A.J. 1941, Leiden Ann. 17, No. 3
Wilson R.E., Devinney E.J. 1971, ApJ 166, 605

This article was processed by the author using Springer-Verlag LaTeX A&A style file *L-AA* version 3.